AIP | Applied Physics Letters

Continuous sheath-free separation of particles by shape in viscoelastic fluids

Xinyu Lu, Lin Zhu, Ri-mao Hua, and Xiangchun Xuan

Citation: Applied Physics Letters **107**, 264102 (2015); doi: 10.1063/1.4939267
View online: http://dx.doi.org/10.1063/1.4939267
View Table of Contents: http://scitation.aip.org/content/aip/journal/apl/107/26?ver=pdfcov
Published by the AIP Publishing

Continuous sheath-free separation of particles by shape in viscoelastic fluids

Xinyu Lu,[1] Lin Zhu,[2] Ri-mao Hua,[3] and Xiangchun Xuan[1,a)]
[1]*Department of Mechanical Engineering, Clemson University, Clemson, South Carolina 29634-0921, USA*
[2]*School of Engineering, Anhui Agricultural University, Hefei, Anhui 230036, China*
[3]*School of Resource and Environment, Anhui Agricultural University, Hefei, Anhui 230036, China*

(Received 17 November 2015; accepted 15 December 2015; published online 29 December 2015)

Shape is an important indicator of cell type, cycle, and state, etc., and can thus serve as a specific marker for label-free bioparticle separation. We demonstrate in this work a shape-based separation of equal-volumed spherical and peanut particles in viscoelastic fluids through straight rectangular microchannels. This continuous sheath-free separation arises from the shape-dependent equilibrium particle position(s) as a result of the flow-induced elasto-inertial lift and shear thinning effects. A continuous transition from single to dual and to triple equilibrium positions is observed for both types of particles with the increase in flow rate. However, the flow rate at which the transition takes place differs with the particle shape. This phenomenon occurs only in microchannels with a large aspect ratio (width/height) and has not been reported before. It is speculated to correlate with the dissimilar dependences of elastic and inertial lift forces on particle size and flow rate as well as the rotational effects of non-spherical particles. © *2015 AIP Publishing LLC*.
[http://dx.doi.org/10.1063/1.4939267]

Shape is an important indicator of cell type,[1] cycle,[2] and state,[3] etc. It provides useful information in, for example, bioparticle identification,[4] cell synchronization,[5] and disease diagnostics,[6] etc. Therefore, shape can be a specific marker for label-free bioparticle separation. It may also serve as a new intrinsic marker for the fractionation of synthetic micro/nanoparticles with immense potential applications in both academics and industry. However, most of current microfluidic techniques have been developed to separate particles by size.[7–10] Only recently the shape-based particle separation has been investigated in a few studies. It can be implemented through hydrodynamic filtration[11] in a complex network of microchannels[12] or through deterministic lateral displacement in high-resolution arrays of posts.[13,14] It has also been demonstrated by the use of dielectrophoresis that can be either electrode-[5] or insulator-based.[15,16] The throughput of this electrical method is, however, very low with the Reynolds number ($Re = \rho V D_h/\eta$, where ρ is the fluid density, V is the average fluid velocity, D_h is the hydraulic diameter, and η is the fluid viscosity) smaller than 0.1. In contrast, differential inertial focusing[17] can separate particles by shape at a high throughput where the Reynolds number must be over 10.[18]

Very recently, our group has demonstrated a continuous separation of equal-volumed spherical and peanut-shaped particles[19] via a method called as elasto-inertial pinched flow fractionation (eiPFF).[20] This method exploits the shape-dependent elasto-inertial lift force in viscoelastic fluids to increase the particle displacement for a high-purity separation at the Reynolds number of order 1. However, a sheath fluid is required to pre-focus the particle mixture which complicates the flow control and dilutes the separated particles. We demonstrate in this work that the flow-induced elasto-inertial lift[21] can direct particles towards shape-dependent equilibrium positions in straight rectangular microchannels for a continuous sheath-free separation at the Reynolds number of order 1. Such a cross-stream particle migration in viscoelastic fluids[22–26] has been recently demonstrated to focus,[27–38] filtrate,[39,40] and separate (by size[41–45] and deformability[46]) particles in microchannels.

We used 4.18 μm-diameter spherical (green fluorescent, Bangs Laboratories, Inc.) and 3.5 μm-diameter/6 μm-length peanut-shaped (plain, Magsphere, Inc.) polystyrene particles to demonstrate the shape-based separation. The peanuts particles have a calculated total volume of 39.84 μm^3, which corresponds to an equivalent spherical diameter of 4.23 μm. The original aqueous suspensions of spherical (1% solid) and peanut-shaped (10% solid) particles were first mixed at a 10:1 ratio and then re-suspended in a polyethylene oxide (PEO) solution to a final concentration of 10^6 particles/ml. Three concentrations of PEO solutions, 500 ppm, 1000 ppm, and 2000 ppm, were prepared by dissolving PEO powder (Sigma-Aldrich, USA; molecular weight of 2×10^6 Da) in water. The particle mixture was also re-suspended in water for a control experiment. A small amount of Tween 20 (0.5% v/v, Fisher Scientific) was added to each prepared particle suspension for the purpose of reducing particle aggregations and adhesions (to channel walls). The rheological properties of the PEO solutions are summarized in Table I. The process for determining their relaxation times are provided in the supplementary material.[47]

Four depths of 2 cm long and 50 μm wide straight rectangular microchannels are used in our experiments, which are 15, 25, 40, and 100 μm, respectively. They were fabricated with polydimethylsiloxane (PDMS) by the standard soft lithography method.[20,48] At the end of each channel, a 2 mm long and 900 μm wide expansion was designed to enhance the particle separation and to facilitate the visualization. The particle suspension was driven through the

a)Author to whom correspondence should be addressed. Electronic mail: xcxuan@clemson.edu. Fax: 864-656-7299.

TABLE I. Rheological properties of the prepared PEO solutions.

Properties (at 20 °C)	PEO solution (c, ppm)		
	500	1000	2000
Zero-shear viscosity η (mPa·s)	1.8	2.3	4.1
Overlap concentration c^* (ppm)	858	858	858
Concentration ratio c/c^*	0.58	1.17	2.33
Zimm relaxation time, λ_{Zimm} (ms)	0.34	0.34	0.34
Effective relaxation time, λ_e (ms)	4.3	6.8	10.6

microchannel by an infusion syringe pump (KDS-100, KD Scientific). Particle motion was recorded through an inverted microscope (Nikon Eclipse TE2000U, Nikon Instruments) with a CCD camera (Nikon DS-Qi1Mc) at a rate of 15 frames/s. Fluorescent and bright-field lights were used simultaneously to identify fluorescent spherical (appear bright) and plain peanut (appear dark) particles. Images were post-processed in Nikon Imaging Software (NIS-Elements AR 3.22). Superimposed images of fluorescent and plain particles were obtained by stacking a sequence of snapshot images (around 800) with the maximum and minimum intensity projections, respectively. The function of particle analysis in ImageJ software package (National Institute of Health) was used to measure the transverse particle positions at the channel outlet (i.e., the channel expansion), which were then used to calculate the probability distribution function (PDF) for each type of particles.

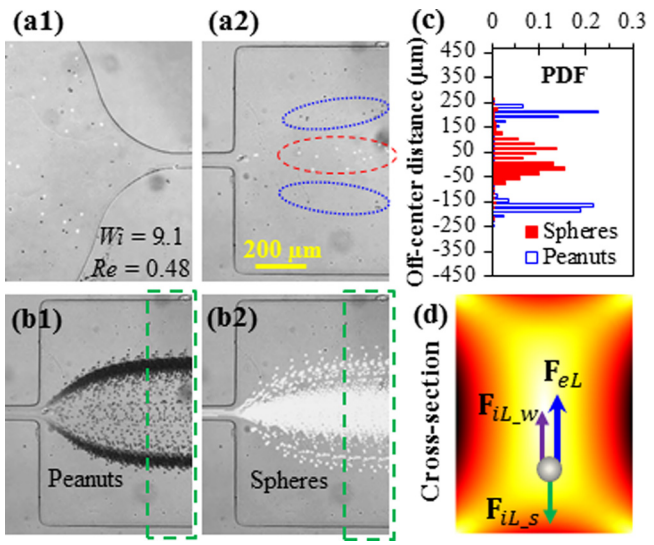

FIG. 1. Demonstration of shape-based separation of plain peanut (dark) and fluorescent spherical (bright) particles in 1000 ppm PEO solution through a 50 μm wide and 25 μm deep straight rectangular microchannel at a flow rate of 150 μl/h: (a1) and (a2) snapshot images at the channel inlet and outlet, respectively, where the broken-line ellipses highlight the separated spherical and peanut particles; (b1) and (b2) superimposed images of peanut and spherical particles at the channel outlet, where the two dashed boxes highlight the regions to be used as cropped images in Figs. 2–4; (c) the plot of particle PDF at the channel outlet; (d) force analysis of elastic lift, $\mathbf{F}_{eL}$, wall-induced inertial lift, $\mathbf{F}_{iL_w}$, and shear gradient-induced inertial lift, $\mathbf{F}_{iL_s}$, on a particle in a viscoelastic fluid flow through a rectangular microchannel, where the background color shows the contour of fluid shear rate (the darker the larger). The flow direction is from left to right in (a1), (a2), (b1), and (b2). (Multimedia view) [URL: http://dx.doi.org/10.1063/1.4939267.1] [URL: http://dx.doi.org/10.1063/1.4939267.2]

Fig. 1 shows the shape-based separation of plain peanut and fluorescent spherical particles in 1000 ppm PEO solution through a 25 μm deep microchannel at a flow rate of 150 μl/h. The two types of particles are uniformly dispersed at the channel inlet in Fig. 1(a1) (Multimedia view) but split to dissimilar streams at the outlet in Fig. 1(a2) (Multimedia view). As viewed from the two superimposed images in Figs. 1(b1) and 1(b2), spherical particles are focused to a single band along the channel centerline, while peanut particles migrate to two equilibrium positions that are each one quarter of the channel width away from the centerline. Such a continuous shape-based separation can be evaluated by the plot of particle PDF in Fig. 1(c), where over 1500 particles are counted for each type. The separation efficiency (defined as the particle percentage at a preferred outlet) is 95.2% and 95.1% for spherical and peanut particles inside and outside the region with an off-center distance of 130 μm in the expansion, respectively. The corresponding separation purity (defined as the ratio of the targeted to the total collected particles at an outlet) is also greater than 95% for each type of particles.

We have also done a control experiment of the same peanut and spherical particles in water under identical conditions (see Fig. S1 in the supplementary material[47]). Neither type of particles experiences a significant inertial focusing because of the small Reynolds number ($Re = 2\rho Q/\eta(w+h) = 1.11$, where Q is the flow rate and w and h are the channel width and height),[49–51] and hence no inertial separation is observed. The Reynolds number is even smaller in the PEO solution [$Re = 0.48$ as labeled in Fig. 1(a1)] due to the increased viscosity. Therefore, our recently demonstrated shape-dependence of the elastic lift,[19] $\mathbf{F}_{eL}$, is the primary reason for the observed particle separation in Fig. 1. As seen from the schematic in Fig. 1(d), $\mathbf{F}_{eL}$ directs particles towards the low-shear-rate regions, i.e., the centerline and four corners of a rectangular channel,[21,29,52] and is characterized by the Weissenberg number ($Wi = \lambda_e\dot{\gamma} = 2\lambda_e Q/w^2h = 9.1$, where λ_e is the effective relaxation time in Table I and $\dot{\gamma}$ is the fluid shear rate). This force competes with the shear gradient-induced inertial lift, $\mathbf{F}_{iL_s}$, and the wall-induced inertial lift, $\mathbf{F}_{iL_w}$, which direct a particle to the chanter wall and center, respectively, as illustrated in Fig. 1(d). The elastic and inertial lift forces are each a positive function of flow rate[21,27,42,53,54] and expressed as follows for particles of (equivalent) spherical diameter a (see the supplementary material[47] for derivations)

$$\mathbf{F}_{eL} \sim \lambda_e (a/w)^3 Q^3, \tag{1}$$

$$\mathbf{F}_{iL} = \mathbf{F}_{iL\_s} + \mathbf{F}_{iL\_w} \sim \rho (a/w)^4 Q^2. \tag{2}$$

Fig. 2 shows the flow rate effect on the shape-based particle separation in 1000 ppm PEO solution through a 25 μm deep microchannel. As the flow rate increases, Re and Wi both increase (see the labeled values on the images) while their ratio, i.e., the elasticity number ($El = Wi/Re = \lambda_e\eta(w+h)/\rho w^2 h$), is independent of flow kinematics and remains at 18.8. At 20 μl/h, peanut and spherical particles are both focused to a stream near the channel centerline except that a small percentage of spherical particles travel near the corner (highlighted by the dashed-line arrows in Fig. 2). Consistent with our earlier studies,[19,20] this secondary equilibrium position disappears at

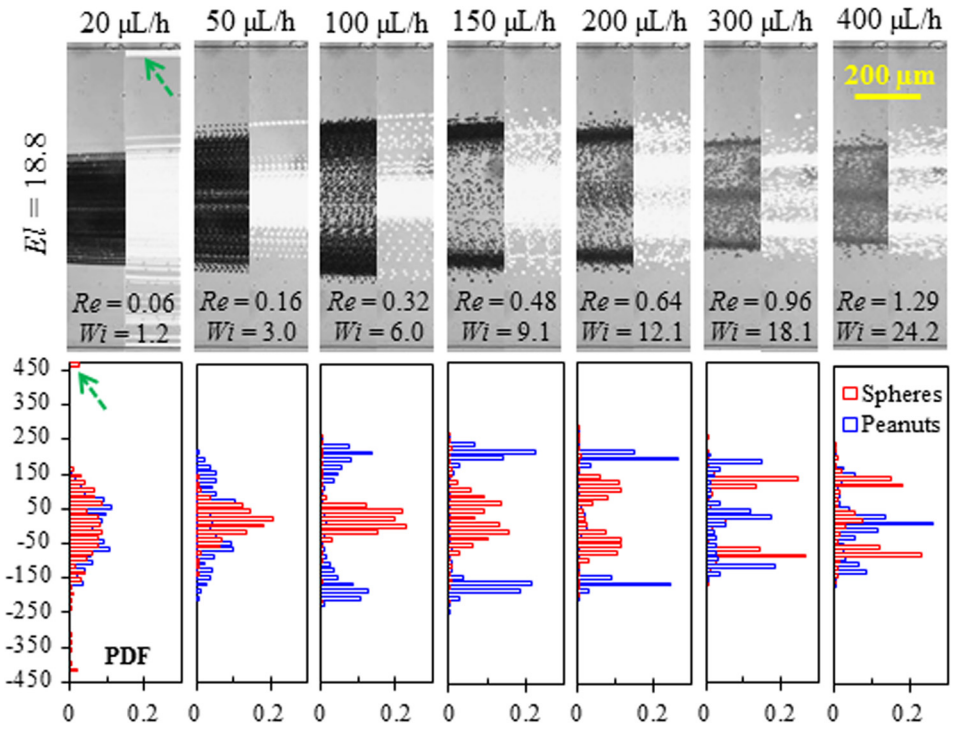

FIG. 2. Flow rate effect (in terms of the Reynolds number, *Re*, and Weissenberg number, *Wi*) on shape-based separation of plain peanut (dark) and fluorescent spherical (bright) particles in 1000 ppm PEO solution through a 50 μm wide and 25 μm deep straight rectangular microchannel: (top row) cropped superimposed particle images at the channel outlet [highlighted by the dashed-line boxes in Figs. 1(b1) and 1(b2)]); (bottom row) plots of particle PDF at the channel outlet. The dashed-line arrows highlight a secondary equilibrium position for spherical particles near the channel corner at a flow rate of 20 μl/h.

higher flow rates and occurs due to the corner-directed elastic lift[21,29,52] under a negligible influence of inertial lift. As the flow rate is increased to 100 μl/h, spherical particles get better focused towards the channel center, while peanut particles instead migrate towards the walls and become split into two streams. This differential elasto-inertial focusing yields the shape-based particle separation, which still holds effective at 150 and 200 μl/h. However, two peaks start occurring for spherical particles in the PDF plot. They grow and move away from the channel center when the flow rate is further increased to 300 μl/h. Meanwhile, however, the two streams of peanut particles shift back towards the channel center, leading to a reduced particle separation. Interestingly, at the flow rate of 300 μl/h (and higher) where *Re* is about 1, an additional equilibrium position appears for each type of particles which eventually breaks down this shape-based separation.

A similar trend can be identified from Fig. 2 for the elasto-inertial focusing between peanut and spherical particles. With the increase in flow rate (or *Re*), each type of particles experiences first a transition from single equilibrium position at the channel centerline to dual equilibrium positions on the two sides of the centerline and then to triple equilibrium positions at both the centerline and its two sides. However, the two transitions for peanut particles both take place at smaller flow rates than for spherical particles, which yields the shape-based separation demonstrated in Figs. 1 and 2. The exact mechanism behind this phenomenon is currently unclear, which is speculated to correlate with the rotational effects of peanut particles. As demonstrated in our earlier study,[19] the preferentially parallel orientation of peanut particles to the flow direction renders the elastic and inertial lift forces more dependent on their shorter dimension (i.e., 3.5 μm) smaller than the diameter of spherical particles (i.e., 4.18 μm). Hence, the dissimilar dependences of $\mathbf{F}_{eL}$ in Eq. (1) and $\mathbf{F}_{iL}$ in Eq. (2) on particle size and flow rate may lead to the observed phenomenon in Fig. 2.

Fig. 3 shows the PEO concentration effect (in terms of the elasticity number, *El*) on the shape-based particle separation in a 25 μm deep microchannel under a fixed flow rate of 150 μl/h. Due to the increased viscosity, *Re* decreases (from 0.62 to 0.48 and 0.27 for 500, 1000, and 2000 ppm) at higher PEO concentrations indicating a weakened inertial lift. In contrast, *Wi* increases due to the extended relaxation time at higher PEO concentrations. The separation is barely visible in 500 ppm PEO because both peanut and spherical particles are still at the state of single equilibrium position along the

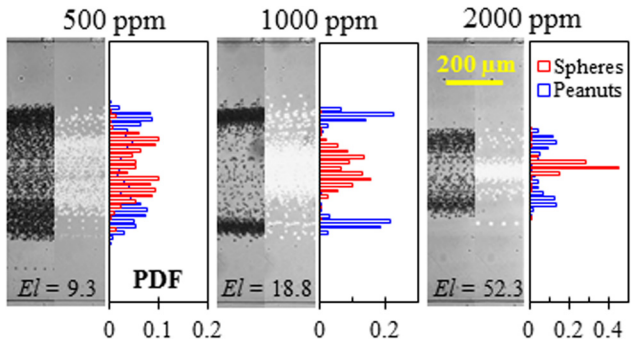

FIG. 3. PEO concentration effect (in terms of the elasticity number, *El*) on shape-based separation of plain peanut (dark) and fluorescent spherical (bright) particles in a 50 μm wide and 25 μm deep straight rectangular microchannels under a flow rate of 150 μl/h. The left and right halves of each panel show the cropped superimposed particle images and the corresponding PDF plots at the channel outlet, respectively.

channel centerline. It is significantly improved in 1000 ppm PEO due to the enhanced elasto-inertial particle focusing, a consequence of the increased elastic lift and the decreased inertial lift. In 2000 ppm PEO, spherical particles experience an improved focusing towards the single equilibrium position along the channel centerline. However, since the two equilibrium positions of peanut particles both shift towards the centerline, the separation gets diminished in 2000 ppm PEO.

We have also studied the flow rate effect on the shape-based particle separation in 500 ppm and 2000 ppm PEO solutions (see Fig. S2 in the supplementary material[47]). Similar to that in Fig. 2, a continuous transition from single to dual and to triple equilibrium positions is found in both PEO concentrations for peanut and spherical particles. Moreover, the two transitions for peanut particles still happen ahead of spherical ones with the increase in low rate. However, the flow rates at which the transitions take place depend on the PEO concentration due to its effect on $\mathbf{F}_{eL}$ in Eq. (1) via the relaxation time, λ_e. This phenomenon is also believed to be related to the enhanced shear thinning effects at higher PEO concentrations, which has been demonstrated in the earlier works[25,26,33,44] to direct particles away from the channel centerline. The best separation in 500 ppm and 2000 ppm PEO (see Fig. S2 in the supplementary material[47]) takes place at 200–300 μl/h and 100–150 μl/h, respectively, which seem consistent with the flow rate of 150–200 μl/h in 1000 ppm PEO (see Fig. 2). Among these three PEO concentrations, 1000 ppm is found to offer the best separation performance in terms of particle PDF.

Fig. 4 shows the effect of channel aspect ratio, $AR = w/h$, on the shape-based particle separation in 1000 ppm PEO solution through microchannels of 40 μm ($AR = 1.25$), 25 μm ($AR = 2.0$), and 15 μm ($AR = 3.3$) deep, respectively. Under a constant flow rate of 150 μl/h, a larger AR corresponds to an increased Re and Wi. In the nearly square microchannel with $AR = 1.25$ (left panel in Fig. 4), peanut and spherical particles are each focused towards the channel centerline. This single equilibrium particle position remains unvaried with the increase in flow rate (up to 1 ml/h), which seems to be consistent with the previous studies in square microchannels ($AR = 1.0$).[34,39,42,44] Since no transition to dual equilibrium positions is observed (see Fig. S3 in the supplementary material[47]), shape-based particle separation is unavailable in a nearly square microchannel. This is also true in a 100 μm deep channel with a low AR (=0.5, data not shown). In the 15 μm deep microchannel with a high AR (=3.3, see the right panel in Fig. 4), peanut particles are focused to three equilibrium positions under a flow rate of 150 μl/h, while spherical particles have only two equilibrium positions. In this high AR microchannel, a transition from single to dual and to triple equilibrium positions still exists for both types of particles (see Fig. S4 in the supplementary material[47]). Moreover, as the transition for peanut particles also happens at a smaller flow rate than for spherical particles, the best separation happens at a flow rate of 50–100 μl/h, which is only one half of that in the 25 μm deep microchannel with $AR = 2.0$.

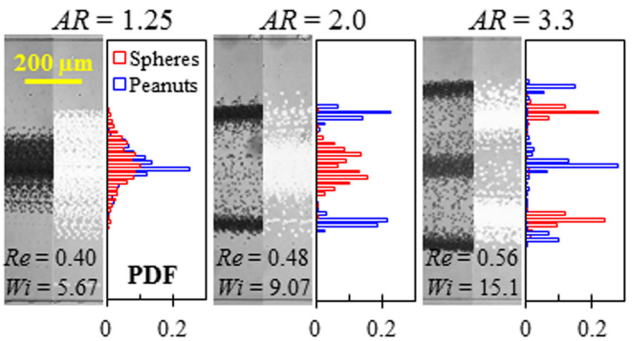

FIG. 4. Channel aspect ratio (AR) effect on shape-based separation of plain peanut (dark) and fluorescent spherical (bright) particles in 50 μm wide straight rectangular microchannels under a flow rate of 150 μl/h. The left and right halves of each panel show the cropped superimposed particle images and the corresponding PDF plots at the channel outlet, respectively.

In summary, we have demonstrated a continuous sheath-free separation of spherical and peanut-shaped rigid particles of equal volume via the elasto-inertial focusing effect in straight rectangular microchannels. This separation exploits the gap between the flow rates at which the two types of particles switch from single to dual equilibrium positions, respectively. It can only take place in large aspect-ratio microchannels, which is $AR \geq 2$ in our tests, because both types of particles migrate towards the single equilibrium position at the centerline of microchannels with an intermediate or low AR. The separation is also found to be strongly dependent on PEO concentration because of its influence on the elastic (via the fluid relaxation time) and inertial (via the fluid viscosity) lifts as well as the shear thinning effects. If necessary, the PEO polymer can be removed by rinsing the separated particle suspension with water or other buffer solutions via centrifugation. Future work will be on the theoretical understanding and numerical prediction of shape-based particle separation in viscoelastic fluids. Moreover, the effects of other experimental parameters such as channel length and polymer type [e.g., polyvinylpyrrolidone (PVP)[39,46] and polyacrylamide (PAA)[27,43]] will be investigated. In addition, we are developing an apparatus to fabricate spheroidal particles of various aspect ratios using the protocol reported earlier[18] for further tests of shape-based particle separation in viscoelastic fluids.

This work was partially supported by NSF under Grant No. CBET-1150670 (X.X.). The support from the National Natural Science Foundation of China (Grant No. 51575003) and the Key Project of Anhui Education Committee (Grant No. KJ2015A031) is also gratefully acknowledged (L.Z.).

[1]S. Mitragotri and J. Lahann, Nat. Mater. **8**, 15 (2009).
[2]S. Martin, Cell Cycle **8**, 3643–3647 (2009).
[3]E. C. Ebert, M. Nagar, and K. D. Hagspiel, Clin. Gastroenterol. Hepatol. **8**, 483–489 (2010).
[4]J. Janca, V. Halabalova, and J. Rzicka, J. Chromatogr. A **1217**, 8062–8071 (2010).
[5]A. Valero, T. Braschler, A. Rauch, N. Demierre, Y. Barral, and P. Renaud, Lab Chip **11**, 1754–60 (2011).
[6]N. M. Anstey, B. Russell, T. W. Yeo, and R. N. Price, Trends Parasitol. **25**, 220–227 (2009).
[7]A. Karimi, S. Yazai, and A. M. Ardekani, Biomicrofluidics **7**, 021501 (2013).
[8]P. Sajeesh and A. K. Sen, Microfluid. Nanofluid. **17**, 1–52 (2014).
[9]Z. T. Yu, K. M. Yong, and J. Fu, Small **10**, 1687–1703 (2014).
[10]C. W. Shields IV, C. D. Reyes, and G. P. Lopez, Lab Chip **15**, 1230–1249 (2015).

[11]M. Yamada and M. Seki, Anal. Chem. **78**, 1357–1362 (2006).
[12]S. Sugaya, M. Yamada, and M. Seki, Biomicrofluidics **5**, 24103 (2011).
[13]J. P. Beech, S. H. Holm, K. Adolfsson, and J. O. Tegenfeldt, Lab Chip **12**, 1048–1051 (2012).
[14]K. K. Zeming, S. Ranjan, and Y. Zhang, Nat. Commun. **4**, 1625 (2013).
[15]Y. Song, J. Yang, X. Shi, H. Jiang, Y. Wu, R. Peng, Q. Wang, N. Gong, X. Pan, Y. Sun, and D. Li, Sci. China **55**, 524–530 (2012).
[16]J. DuBose, X. Lu, S. Patel, S. Qian, S. W. Joo, and X. Xuan, Biomicrofluidics **8**, 014101 (2014).
[17]S. C. Hur, S. E. Choi, S. Kwon, and D. Di Carlo, Appl. Phys. Lett. **99**, 044101 (2011).
[18]M. Masaeli, E. Sollier, H. Amini, W. Mao, K. Camacho, N. Doshi, S. Mitragotri, A. Alexeev, and D. Di Carlo, Phys. Rev. X **2**, 031017 (2012).
[19]X. Lu and X. Xuan, Anal. Chem. **87**, 11523–11530 (2015).
[20]X. Lu and X. Xuan, Anal. Chem. **87**, 6389–6396 (2015).
[21]G. D'Avino and P. L. Maffettone, J. Non-Newtonian Fluid Mech. **215**, 80–104 (2015).
[22]A. Karnis, H. L. Goldsmith, and S. G. Mason, Nature **200**, 159–160 (1963).
[23]B. P. Ho and L. G. Leal, J. Fluid Mech. **76**, 783–799 (1976).
[24]G. Leal, J. Non-Newtonian Fluid Mech. **5**, 33–78 (1979).
[25]P. Y. Huang, J. Feng, H. H. Hu, and D. D. Joseph, J. Fluid Mech. **343**, 73–94 (1997).
[26]P. Y. Huang and D. D. Joseph, J. Non-Newtonian Fluid Mech. **90**, 159–185 (2000).
[27]A. M. Leshansky, A. Bransky, N. Korin, and U. Dinnar, Phys. Rev. Lett. **98**, 234501 (2007).
[28]G. D'Avino, G. Romeo, M. Villone, F. Greco, P. A. Netti, and P. L. Maffettone, Lab Chip **12**, 1638–1645 (2012).
[29]J. Y. Kim, S. W. Ahn, S. S. Lee, and J. M. Kim, Lab Chip **12**, 2807–2814 (2012).
[30]S. Cha, T. Shin, S. S. Lee, W. Shim, G. Lee, S. J. Lee, Y. Kim, and J. M. Kim, Anal. Chem. **84**, 10471–10477 (2012).
[31]D. L. Lee, H. Brenner, J. R. Youn, and Y. S. Song, Sci. Rep. **3**, 3258 (2013).
[32]F. D. Giudice, G. Romeo, G. D'Avino, F. Greco, P. A. Netti, and P. L. Maffettone, Lab Chip **13**, 4263–4271 (2013).
[33]K. W. Seo, H. J. Byeon, H. K. Huh, and S. J. Lee, RSC Adv. **4**, 3512–3520 (2014).
[34]E. J. Lim, T. Ober, J. F. Edd, S. P. Desai, D. Neal, K. W. Bong, P. S. Doyle, G. H. McKinley, and M. Toner, Nat. Commun. **5**, 4120 (2014).
[35]S. Cha, K., Kang, J. B. You, S. G. Im, Y. Kim, and J. M. Kim, Rheol. Acta **53**, 927–933 (2014).
[36]K. W. Seo, Y. R. Ha, and S. J. Lee, Appl. Phys. Lett. **104**, 213702 (2014).
[37]F. D. Giudice, G. D'Avino, F. Greco, P. A. Netti, and P. L. Maffettone, Microfluid. Nanofluid. **19**, 95–104 (2015).
[38]D. Yuan, J. Zhang, S. Yan, C. Pan, G. Alici, N. T. Nguyen, and W. H. Li, Biomicrofluidics **9**, 044108 (2015).
[39]S. Y. Yang, J. Y. Kim, S. J. Lee, S. S. Lee, and J. M. Kim, Lab Chip **11**, 266–273 (2011).
[40]S. W. Ahn, S. S. Lee, S. J. Lee, and J. M. Kim, Chem. Eng. Sci. **126**, 237–243 (2015).
[41]J. Nam, H. Lim, D. Kim, H. Jung, and S. Shin, Lab Chip **12**, 1347–1354 (2012).
[42]K. Kang, S. S. Lee, K. Hyun, S. J. Lee, and J. M. Kim, Nat. Commun. **4**, 2567 (2013).
[43]H. Lim, J. Nam, and S. Shin, Microfluid. Nanofluid. **17**, 683–692 (2014).
[44]C. Liu, C. Xue, X. Chen, L. Shan, Y. Tian, and G. Hu, Anal. Chem. **87**, 6041–6048 (2015).
[45]J. Nam, B. Namgung, C. T. Lim, J. Bae, H. L. Leo, K. S. Cho, and S. Kim, J. Chromatogr. A **1406**, 244–250 (2015).
[46]S. Yang, S. S. Lee, S. W. Ahn, K. Kang, W. Shim, G. Lee, K. Hyune, and J. M. Kim, Soft Matter **8**, 5011–5019 (2012).
[47]See supplementary material at http://dx.doi.org/10.1063/1.4939267 for the determination of PEO solution properties, control experiment of shape-based particle separation in water, derivation of Eqs. (1) and (2), and flow rate effects on shape-based particle separation in different PEO solutions through microchannels of different aspect ratios.
[48]X. Lu, S. Patel, M. Zhang, S. Joo, S. Qian, A. Ogale, and X. Xuan, Biomicrofluidics **8**, 021802 (2014).
[49]H. Amini, W. Lee, and D. Di Carlo, Lab Chip **14**, 2739–2761 (2014).
[50]J. M. Martel and M. Toner, Annu. Rev. Biomed. Eng. **16**, 371–396 (2014).
[51]J. Zhang, S. Yan, D. Yuan, G. Alici, N. T. Nguyen, M. E. Warkiani, and W. Li, Lab Chip **16**, 10–34 (2016).
[52]K. W. Seo, Y. J. Kang, and S. J. Lee, Phys. Fluids **26**, 063301 (2014).
[53]E. S. Asmolov, J. Fluid Mech. **381**, 63–87 (1999).
[54]D. Di Carlo, J. F. Edd, K. J. Humphry, H. A. Stone, and M. Toner, Phys. Rev. Lett. **102**, 094503 (2009).